Reprinted from:
Journal of Imaging Science and Technology® 59(4): 040401-1–040401-10, 2015.

Aerodynamic Effects in Industrial Inkjet Printing

Cristina Rodriguez-Rivero, José Rafael Castrejón-Pita, and Ian M. Hutchings
University of Cambridge, Department of Engineering, 17 Charles Babbage Rd, Cambridge CB3 0FS, UK
E-mail: mcr51@cam.ac.uk

Abstract. *The quality achieved by inkjet printing is limited by various factors, including the nozzle–substrate throw distance, the substrate velocity, and the occurrence of satellite droplets. Under certain conditions, particularly for large throw distances, unacceptable inaccuracies and defects in drop placement occur. In this paper, a new technique based on high-speed imaging and laser optics is presented that allows the visualization of air currents and droplet movement patterns beneath and in the proximity of a printhead and a moving substrate. The images obtained with this technique provide better temporal and spatial resolution than those obtained in previous studies. Tests with two different commercial printheads show that the entrained airflow depends on the interaction with the stream of printed droplets. The formation of unsteady eddies, particularly between nozzle rows, can result in serious errors in drop placement.* © *2015 Society for Imaging Science and Technology.*
[DOI: 10.2352/J.ImagingSci.Technol.2015.59.4.040401]

INTRODUCTION

Inkjet processes encountered in industrial environments comprise the generation and deposition of micrometric-sized droplets on to a printing medium which normally moves at a constant speed relative to the printhead. It has been observed that the throw distance between the printhead and substrate, and the velocity of the moving medium, strongly influence the print quality. Commercially available systems are commonly restricted to operate with throw distances—referred to below as *gaps*—of the order of 1–2 mm, which can limit the applications of inkjets in markets other than graphics. In order to widen the use of this technology to new applications, one of the priorities is to increase the gap without compromising the printing quality.

The dynamics of the very small droplets produced by commercial printheads are susceptible to the influence of air currents, turbulence, and environmental conditions found within the gap. Aerodynamic forces thus become very important in the precise deposition of the droplets, and great efforts are being made in finding ways to control and reduce their negative effects. It is generally accepted that the airflows between the printhead and substrate are not well characterized and that the reasons that cause airflow-related printing defects are not well understood.

In recent years, a few studies describing and examining the airflow under a printhead have been published. Link et al.[1] studied aerodynamic effects in terms of the substrate velocity for a fixed gap of 2 mm. They investigated the airflow in the gap with particle image velocimetry (PIV) analyses and computational simulations. Numerical studies predicted the formation of vortices close to the substrate, these being responsible for inaccuracies in the deposition of the droplets. Unfortunately, they were unable to investigate this region of interest due to experimental difficulties and the limited resolution of their imaging setup. However, they experimentally confirmed the development of a standard Couette flow in the gap, and used that to validate computational simulations. Hsiao et al. published two papers on the topic, the first on the effect of the substrate speed on a single jetted drop[2] and the second on the effect of the gap distance on the quality of printing.[3] In their first study, high-speed visualization and particle tracking were used to confirm the existence of a standard Couette airflow in a 2 mm gap. They concluded that the effect of the gap airflow was negligible on the dynamics of the jetted drop and ligament deflection, and found an observable interaction between the wake generated by the droplets and the airflow in the gap. In the second work, Hsiao et al.[3] performed experiments with a two-row multi-nozzle printhead to study the effect of the gap—from 2 to 5 mm—on the generation of printing defects, and applied image analysis to the printed patterns. From tests performed with a frontal air guard mounted on a printhead, they concluded that aerodynamic effects have a much greater effect on drops from one row than from the other, and that the interaction between wakes and the entrained flow influences droplet directionality.

The final work on the topic of aerodynamic effects on droplets was that of Barnett and McDonald,[4] who varied both the gap (from 2.5 to 5.1 mm) and the substrate speed. Their study was focussed on the interaction between the wakes and the entrained Couette flow. In this work, high-speed shadowgraphy was used to study the flow between the printhead and the substrate. The conclusion was that the inertia of the Couette flow within the gap determines droplet directionality. They tracked smoke particles from shadowgraph images, and observed the generation of vortices upstream from the jetted droplets, which was confirmed by computational simulations.

All these previous studies have shed light on possible causes for the occurrence of printing defects, but there is still much to be done in the study of the aerodynamics of jetted droplets. Experimental systems are often dedicated to obtaining images so that only qualitative data is produced. As a consequence, the detailed behavior of the airflow in the gap

Received Apr. 9, 2015; accepted for publication June 1, 2015; published online July 10, 2015. Associate Editor: Kye-Si Kwon.
1062-3701/2015/59(4)/040401/10/$25.00

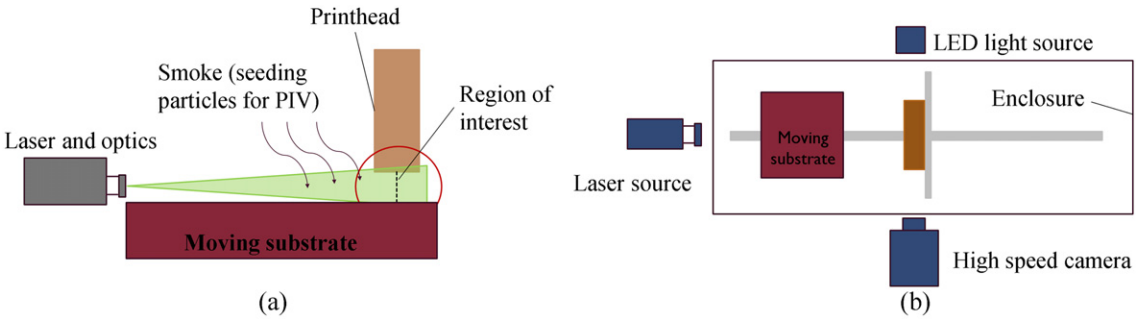

Figure 1. Schematic views of the experimental setup: (a) side view and (b) top view.

is still not fully understood for various printhead gaps. In this paper, we describe an experimental rig in which velocimetry techniques are used in conjunction with image analysis tools to extract the airflow dynamics within the gap. The approach is based on high-speed imaging and laser visualization. The technique has great potential, and it may be applied to a wide range of printhead geometries and experimental conditions. Time-resolved particle image velocimetry (t-PIV) analysis was also used to study the airflow between the printhead and the substrate quantitatively for various conditions: the substrate speed, printing frequency, droplet size, gap size, and number and location of printing rows were investigated, mainly to replicate the conditions in current industrial applications. Our results identify the range of conditions for defective and satisfactory printing.

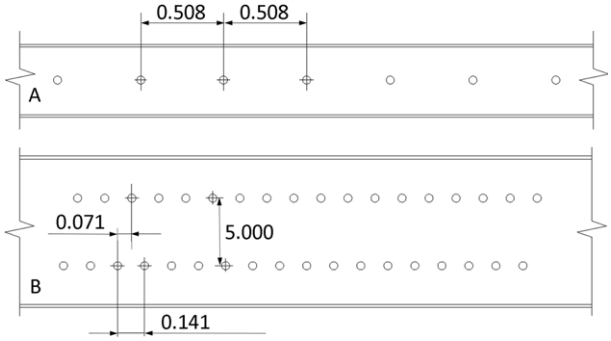

Figure 2. Schematic view of the printheads, with dimensions in millimeters. (a) Single-row printhead, (b) double-row printhead. The drawing is not to scale.

EXPERIMENTAL SETUP

The experimental setup consisted of various illumination and optical components, a printhead, and a linearly moving substrate. Two visualization arrangements were used: a time-resolved particle image velocimetry (t-PIV) system and a high-speed shadowgraph setup. The former system consisted of a continuous diode laser (500 mW, 532 nm) coupled to a 10 mm focal length planoconvex cylindrical lens (310 YD 25, Comar Optics) to create a laser sheet. The waist of the laser was taken, from the manufacturer's specifications, to be 800 μm. Consequently the laser sheet had the same thickness. The cylindrical lens was placed 34 cm away from the center of the printhead so as to diverge the beam enough to cover the desired field of view (up to 67 × 32 mm). The rest of the PIV system consisted of a Phantom V310 high-speed camera and a smoke generator. For shadowgraph illumination, a 100 W light-emitting diode (LED) array with a light diffuser was placed behind the printhead aligned to the camera. A 90 mm macro lens (Tamron) was used on the camera for both visualization modes. The iris settings of the lens were adjusted to control the depth of field, which ranged from 1 mm for laser illumination to ∼10 mm for shadowgraph. A motorized stage was used for all the experiments presented here, comprising a linear motor (model TB2506 with Xenus XSL amplifier, Copley Controls) and a linear encoder system (Renishaw RGH22, with tape scale RGS20-S); the 200 mm × 200 mm moving platform carried a flat paper substrate beneath the fixed printhead. The arrangement of these components can be seen in Figure 1.

Experiments were performed with two different commercial drop-on-demand printheads: a single-row printhead of 128 nozzles with nozzle pitch of 508 μm (referred to as printhead A hereafter), and a double-row printhead of 1000 nozzles with nozzle pitch 70.5 μm (referred to as printhead B hereafter). The characteristic dimensions are shown in Figure 2. Printhead A was fed with black UV-curable ink and printhead B with brown UV-curable ink. Printhead A was controlled by a commercial driver which permitted adjustment of the printing frequency and the speed of printing. Printhead B was driven by a controller working at 6 kHz printing frequency with a variable droplet size (gray levels).

Tests were performed by firing 20 central nozzles of printhead A while varying the substrate velocity, gap distance, and printing frequency. Parametric studies with printhead B involved firing either 60 central nozzles, or an entire nozzle row (of 500 nozzles), or the whole two-row array of 1000 nozzles while varying the substrate velocity, the gap distance, and the droplet size.

RESULTS

As mentioned above, the substrate velocity, gap, frequency, and droplet size were varied to assess the printhead performance in terms of the airflow behavior. Conditions relevant

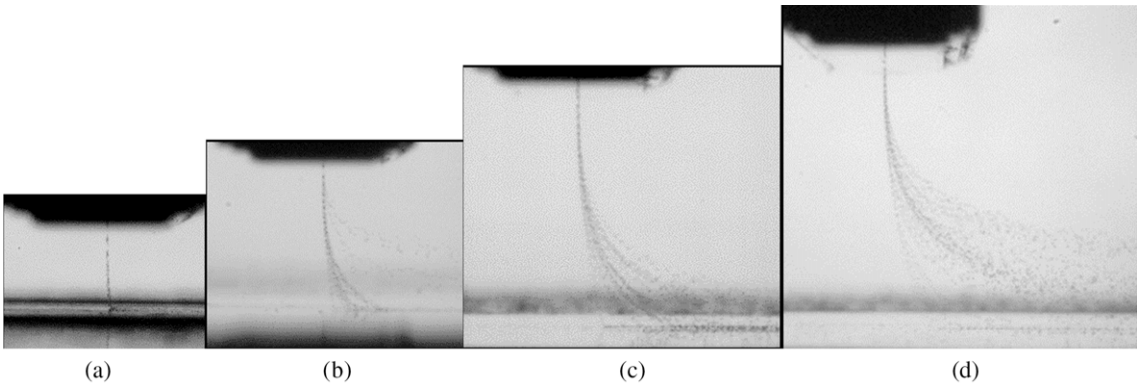

Figure 3. Shadowgraph images of jetting at different gap distances: (a) 3 mm, (b) 5 mm, (c) 7 mm, and (d) 9 mm. Substrate motion is from left to right at 0.5 m/s at a printing frequency of 8 kHz. These images correspond to printhead A jetting from 20 central nozzles only.

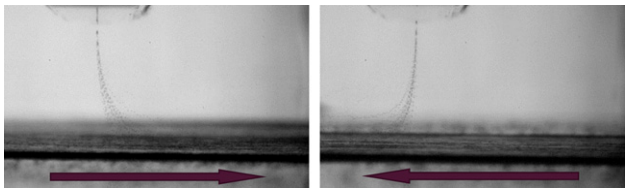

Figure 4. Shadowgraph images showing the deviation of jetted droplets at 5 kHz and a gap distance of 7 mm for a substrate speed of 0.5 m/s (moving direction as indicated by the arrow). Printhead A jetting from 20 central nozzles only.

for both current and potential industrial applications were examined. The ranges of these parameters were as follows.

- Substrate velocity: 0 to 1 m/s
- Gap: 3 to 9 mm (printhead A)/1 to 7 mm (printhead B)
- Printing frequency: 1 to 10 kHz (A)/6 kHz (B)
- Droplet volume: 20 pL (A)/13 and 63 pL (B)
- Droplet velocity: 7 m/s (A)/6 m/s (B)

High-speed shadowgraph imaging, laser visualization, and printed patterns were recorded in all the experiments. Shadowgraph images were captured at 40,000 frames per second (fps) with a 10 μs exposure time. Laser visualization images were recorded over a range from 1500 to 4000 fps (dependent on the substrate speed and light scattering properties of the ink droplets) with exposure times from 999 to 330 μs. The full power of the laser was used in all the experiments to reduce the exposure time of individual frames. In fact, the exposure time in our setup was limited by the power of the laser, the numerical aperture of the lens and the sensitivity of the charge-coupled device (CCD) sensor of the high-speed camera. Experiments at higher substrate speeds than the ones explored in this work will require the improvement of all these three factors.

Figures 3 and 4 show shadowgraph images for printhead A. These show the effect of increasing the gap and changing the direction of motion of the substrate. Fig. 3 shows the deviation suffered by the droplets as the gap increases. Fig. 4 demonstrates that the direction of the substrate motion does not play a major role in the droplet directionality or drag, as no preferential direction is observed. Figs. 3 and 4 also illustrate how droplets and satellite droplets produced by individual nozzles behave differently.

System A permitted a parametric study of gap distances, printing frequencies, and substrate speeds. In contrast, system B allowed the adjustment of gap distances and substrate speeds for a fixed printing frequency of 6 kHz. Another adjustable parameter in both systems was the timing of both the start of printing and the start of image recording, in order to study the differences between starting the printing at the edge, middle, or end of the moving substrate. Examples of these experiments are shown in Figure 5, where three behaviors are clearly distinguished: (a) initiating the printing close to the edge introduces extensive boundary dynamics that alters droplet directionality, (b) printing during the development of the Couette flow within the gap produces an unsteady drag of droplets along the direction of the substrate motion, and (c) the gap dynamics completely develops and

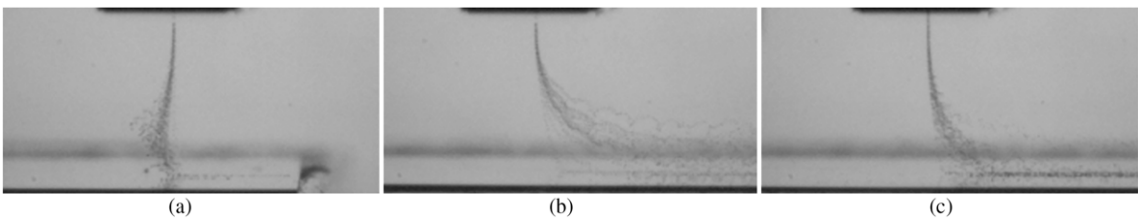

Figure 5. Shadowgraphs showing the behavior of jetted droplets at 10 kHz and a thrown distance of 5 mm for a substrate speed of 1 m/s. Printhead A ejecting 20 central lines.

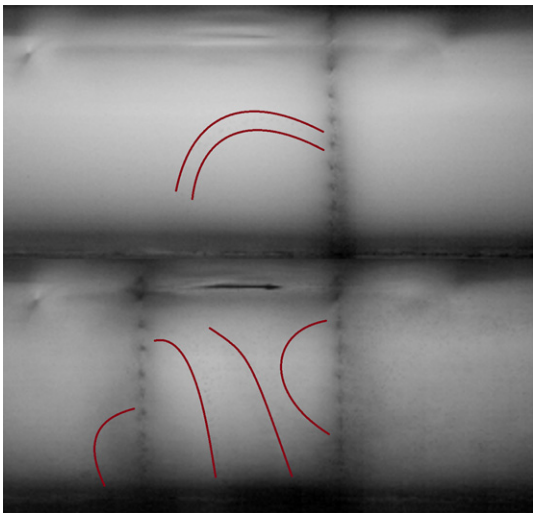

Figure 6. Shadowgraph images for the printing at a 5 mm gap with a substrate speed of 0.12 m/s with 13.1 pL droplets (top image: second row alone; bottom image: two-row printing). Printhead B.

the jet stabilizes directionally, showing a steady and less pronounced deviation in the printed droplets.

As discussed elsewhere,[4] the nozzle pitch can have a major influence on droplet directionality. This is normally observed in printed patterns in which printheads with smaller nozzle spacing result in more defects than printheads with smaller nozzle pitch. This suggests that more closely spaced drops interact more strongly with their neighbors, altering the dynamics of their surroundings. To investigate this aspect, experiments were performed with printhead B by printing from the complete array of 1000 nozzles. Under these conditions, imaging of the entire nozzle array is poor, as in order to capture as much light as possible a wide aperture is needed, which results in a small depth of field. The images recorded therefore appear blurred, with drops behind and in front of the focal plane being out of focus. Figure 6 shows two images with either an individual row or two rows printing under the same conditions. Differences can be observed for these two cases: for single-row printing the stream of droplets generates an eddy flow that goes upwards, toward the nozzle plate, while the dynamics of two-row printing shows complex recirculation of satellite droplets within the space between the rows.

Figure 7 contrasts the shadowgraph and laser visualization methods; for the latter, a laser sheet and smoke particles were used. Laser imaging highlights the satellite dynamics well, as these smaller particles also produce light scattering. Both satellite droplets and smoke particles permit the use of t-PIV analysis. Open-source software (PIVLab) running in MatLab was used for the PIV analysis. Velocity fields and complementary data such as vorticity or velocity divergence can be readily obtained. Generally, the field of view of the raw images was 67 × 32 mm (1280 × 600 pixels), with a resolution of 19.1 pixel/mm. The size of the field analyzed by t-PIV was reduced to cover a smaller region of interest, with sizes ranging from 67 × 16 mm to 23 × 7 mm. The algorithm used for the analysis was a multi-pass fast Fourier transform (FFT) with window deformation, with four passes ranging over interrogation areas from 64 to 16 pixels (3.4 to 0.84 mm with 50% of window overlap). Static masking was used over specific image areas, i.e., the printhead and the substrate, when required.

Fig. 7 also shows the velocity vectors extracted by the PIV analysis for the three different cases shown in Fig. 5. The analysis shows the initial disruption of the jet of droplets due to the vortex created as the substrate platform enters the zone below the printhead. PIV analyses of the second and third cases show an increasing stabilization of the flow, first displaying the effects of high air speeds which exert pronounced drag on the droplets, and later developing into a steady laminar Couette flow.

With the present experimental setup, the nozzle pitch (508 μm) and laser sheet width (∼800 μm) permitted the

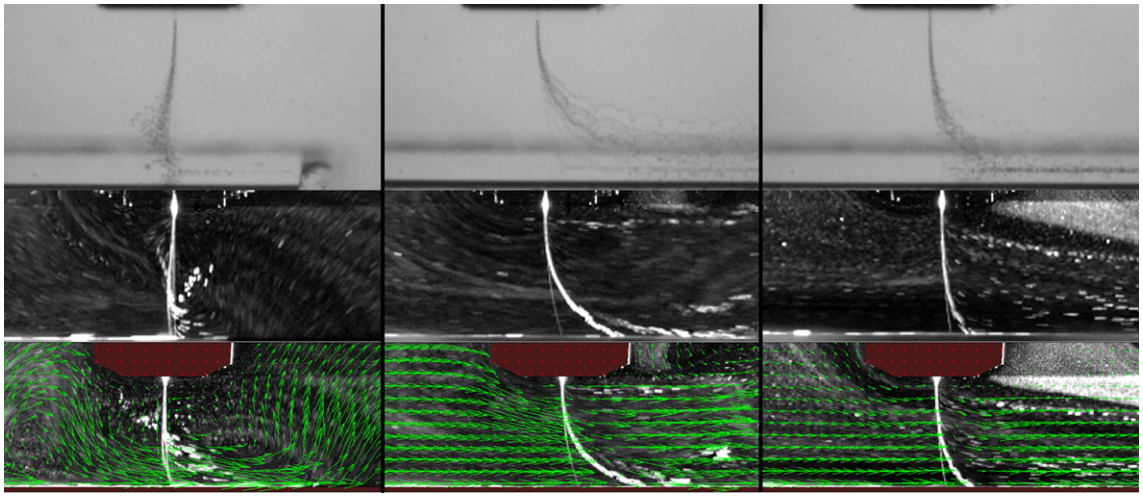

Figure 7. Investigation of satellite motion and airflows. Upper row: shadowgraphy; middle row: laser visualization; bottom row: velocity vectors extracted from t-PIV analysis. Printing conditions: 5 mm gap, 1 m/s substrate speed, 10 kHz ejection frequency. Printhead A ejecting 20 central lines.

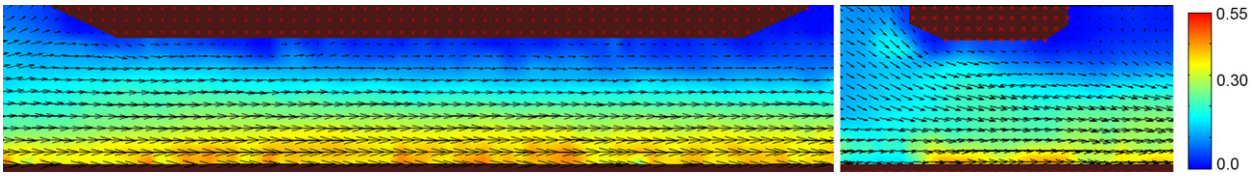

Figure 8. Developed airflow under the printheads (printhead B at the left and printhead A at the right) for a 5 mm gap.

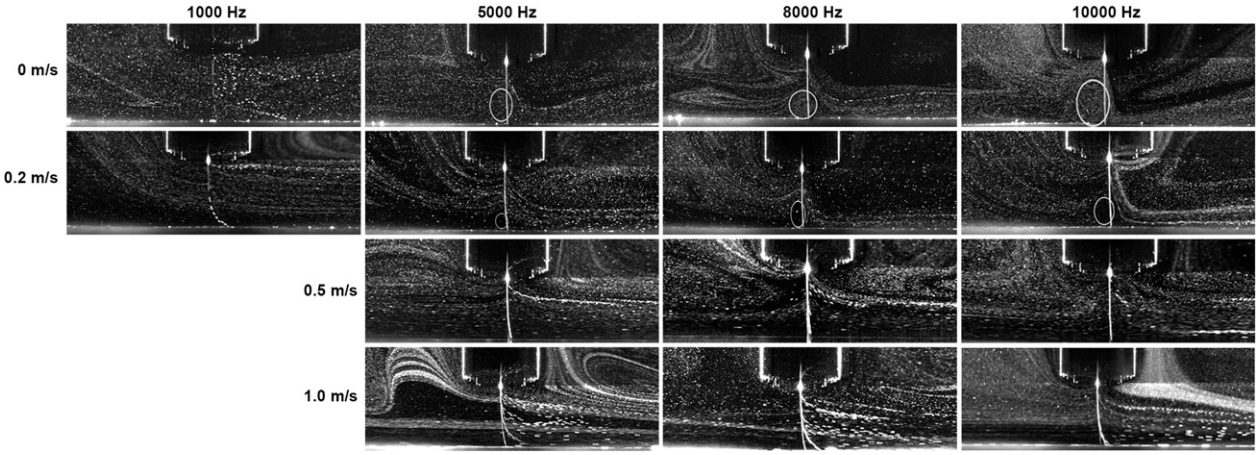

Figure 9. Airflow and satellite motion under different printing conditions for a constant gap of 5 mm. Printhead B. The conditions where an upstream eddy is formed are marked with gray ellipses.

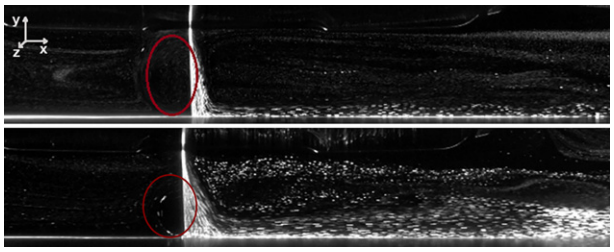

Figure 10. Airflow and satellite motion for a substrate speed of 0.55 m/s, 13.1 pL droplets, and 5 mm gap, firing 30 nozzles (top image) and 500 nozzles (bottom). Printhead B.

illumination of drops from either one or two printing nozzles. This versatility allowed the examination of individual or pairs of drop sequences by scanning the laser along the nozzle array. As mentioned before, the temporal and spatial resolution of the experimental array, as with any other t-PIV system, was mainly determined by the power of the laser and the sensitivity of the camera.

DISCUSSION

In an initial set of experiments, the airflow developed under the two different printheads was studied. Figure 8 compares the flow for both printheads at a substrate speed of 0.55 m/s, with a gap of 5 mm and no jetting. The dynamics under printhead B develops into a full Couette flow. In contrast, given its shorter nozzle plate width, the gap flow under printhead A does not develop into a full Couette flow.

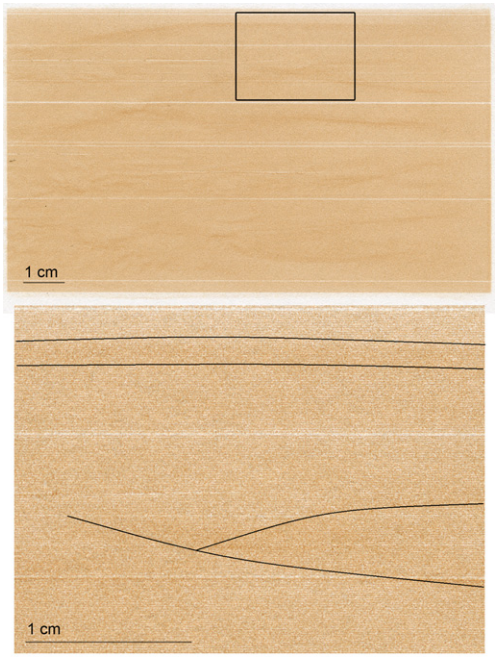

Figure 11. Printed pattern obtained from 500 nozzles firing in a single row for a substrate speed of 0.55 m/s, 13.1 pL droplets, and 5 mm gap. The substrate motion was toward the right. Bottom: the delimited region is displayed in more detail.

The flows presented in Fig. 8 are disrupted both by the introduction of streams of droplets and by increasing the speed of the substrate. Figure 9 shows these effects for printhead A. In this figure, the substrate speed is varied from

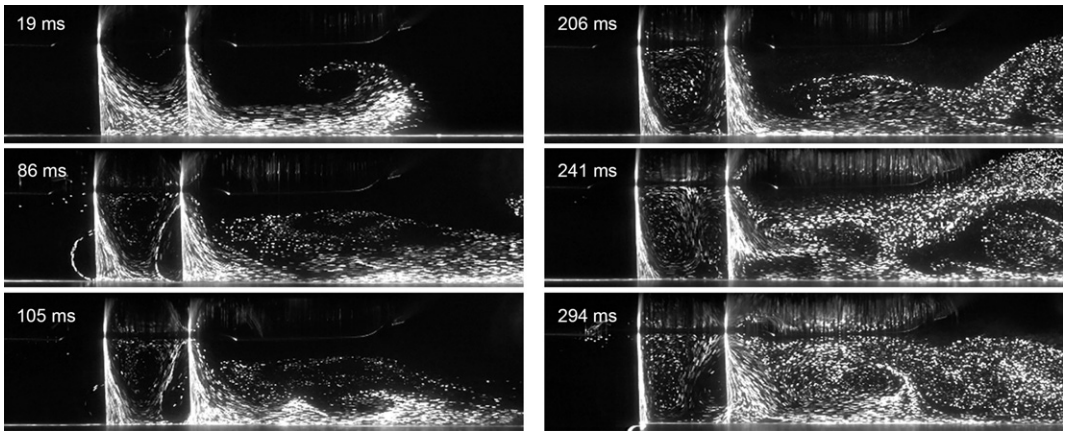

Figure 12. Satellite motion for a substrate speed of 0.12 m/s, 13.1 pL droplets, and 5 mm gap firing 1000 nozzles in two rows. Referred times take zero reference as the start of printing. Smoke seeding particles were not used for these images.

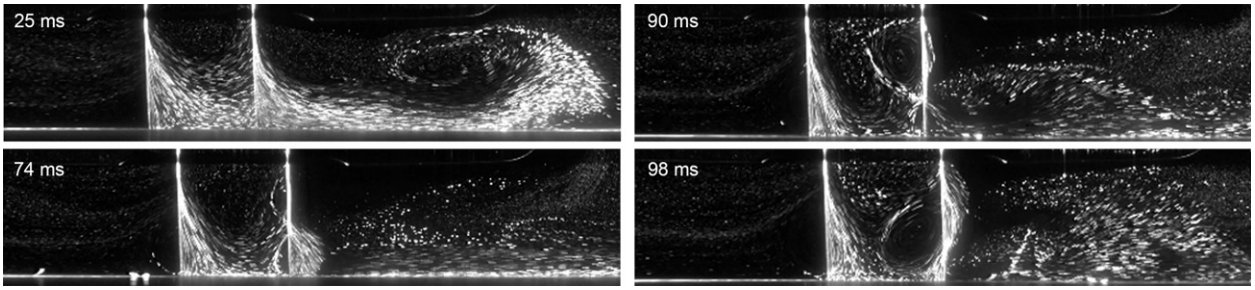

Figure 13. Air and satellite motion for a substrate speed of 0.55 m/s, 13.1 pL droplets, and 5 mm gap firing 1000 nozzles in two rows. Referred times take zero reference as the start of printing.

zero to 1.0 m/s for a fixed gap (5 mm). For low printing frequencies (1 kHz), the spacing of the droplets is such that the interaction between the entraining airflow and the droplets is too small to develop any important disruption to the Couette flow. However, the droplets (main and satellites) are dragged downstream and laterally, increasing droplet misplacement and reducing the resolution.

As expected, as the droplet number increases, by increasing the printing frequency, the flow disruption also increases. In fact, for low substrate speeds, an upstream eddy flow develops that becomes larger for increasing printing frequencies. This effect could be canceled out by use of higher substrate velocities, where inertia eliminates this phenomenon to regain Couette conditions.

The role of the number of nozzles firing and their effect on the gap flow were also studied. Figure 10 shows the ejection of droplets from a single row of printhead B under the same conditions except the number of active nozzles. When 30 nozzles were fired, the flow of droplets downstream remained steady. In contrast, when the whole line array of 500 nozzles was fired, a much more disrupted flow downstream was observed, and a large number of satellites remained as mist under the printhead. In both cases—30 and 500 nozzles—satellites from neighboring nozzles can be seen crossing the field illuminated by the laser, which suggests that a cross-flow was developed along the nozzle array. This effect is much more noticeable at the ends of the printhead, where deposition is known to be greatly affected, as seen in Figure 11. This indicates that droplets and satellites

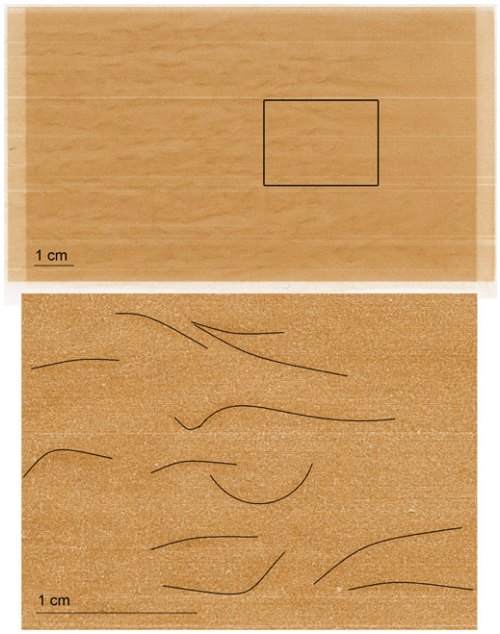

Figure 14. Printed pattern obtained from 1000 nozzles firing in two rows for a substrate speed of 0.55 m/s, 13.1 pL droplets, and 5 mm gap. The substrate motion was toward the right. Bottom: the delimited region is displayed in more detail.

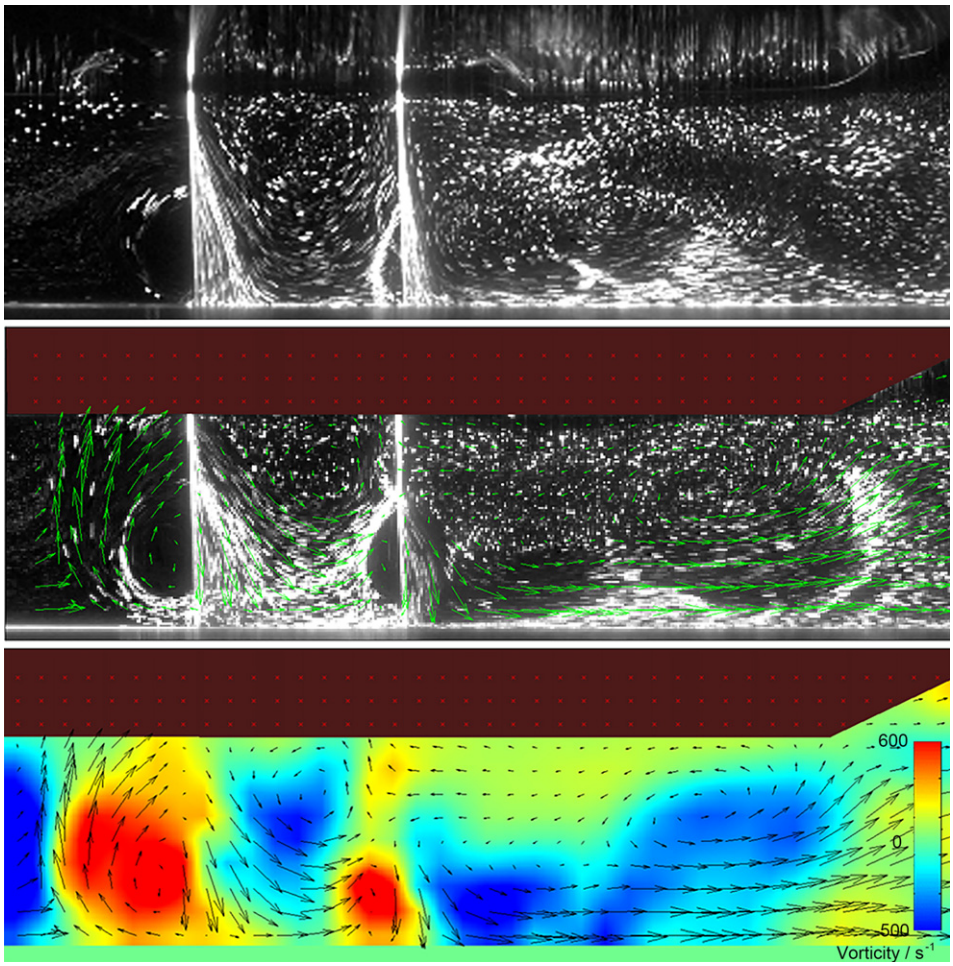

Figure 15. The t-PIV results for 1000 nozzles ejecting from two rows for a substrate speed of 0.55 m/s, 13.1 pL droplets, and 5 mm gap. The substrate moved toward the right.

interact not only with the entrained airflow but also with the wakes. The jetted droplets exchange momentum with the surrounding air and induce a vertical airflow accompanying the stream. Beulen et al.[5] studied the flows on a printhead nozzle plate, and they found the development of these vertical air wakes to be one of the causes. They confirmed that the wakes generated by the droplets are strong enough to influence the surroundings of the stream of droplets. From the current work we suggest that wakes could also promote neighboring nozzle misbehavior, too.

Fig. 11 shows the results of 500 nozzles of a single-row printing continuously at 6 kHz onto a paper substrate moving at 0.55 m/s. Optical microscopy can easily assess the drop and satellite misplacement along the pattern. These observations confirm that drop placement defects continuously build up during printing, and also corroborate the occurrence of a lateral flow that affects the drop and satellite directionality and deposition. It is important to note that in this case the printed pattern also shows missing lines, due to nozzle blockage.

In further experiments with printhead B, the whole two-line nozzle array was fired. Figure 12 shows the interaction between these two rows of nozzles while printing at 6 kHz. Smoke particles were not used, in order to study only the motion of main and satellite droplets. From the early stages the satellites are seen to be trapped under the printhead array, and they remain trapped for the whole printing process. The initial motion of the satellites between rows is unstable, which results in the formation of unsteady eddies. The entrainment of satellites from neighboring lines is again clear.

Figure 13 shows conditions more similar to those found in industrial applications, i.e., with a substrate speed of 0.55 m/s. In this case, a similar pattern is observed to that seen above in the early stages of printing, where a central eddy develops under the printhead close to the nozzle array, leading the satellites from the first row to the second row. This inner eddy close to the nozzle plate grows with time and eventually gives way, once again, to the formation of competing eddies. It is noticeable that one of these eddies forms close to the nozzle plate and shifts toward the substrate, sweeping along satellites when approaching the substrate, as observed in the second image of Fig. 13.

Experiments suggest that the eddy shedding has a particular frequency of formation that depends on the

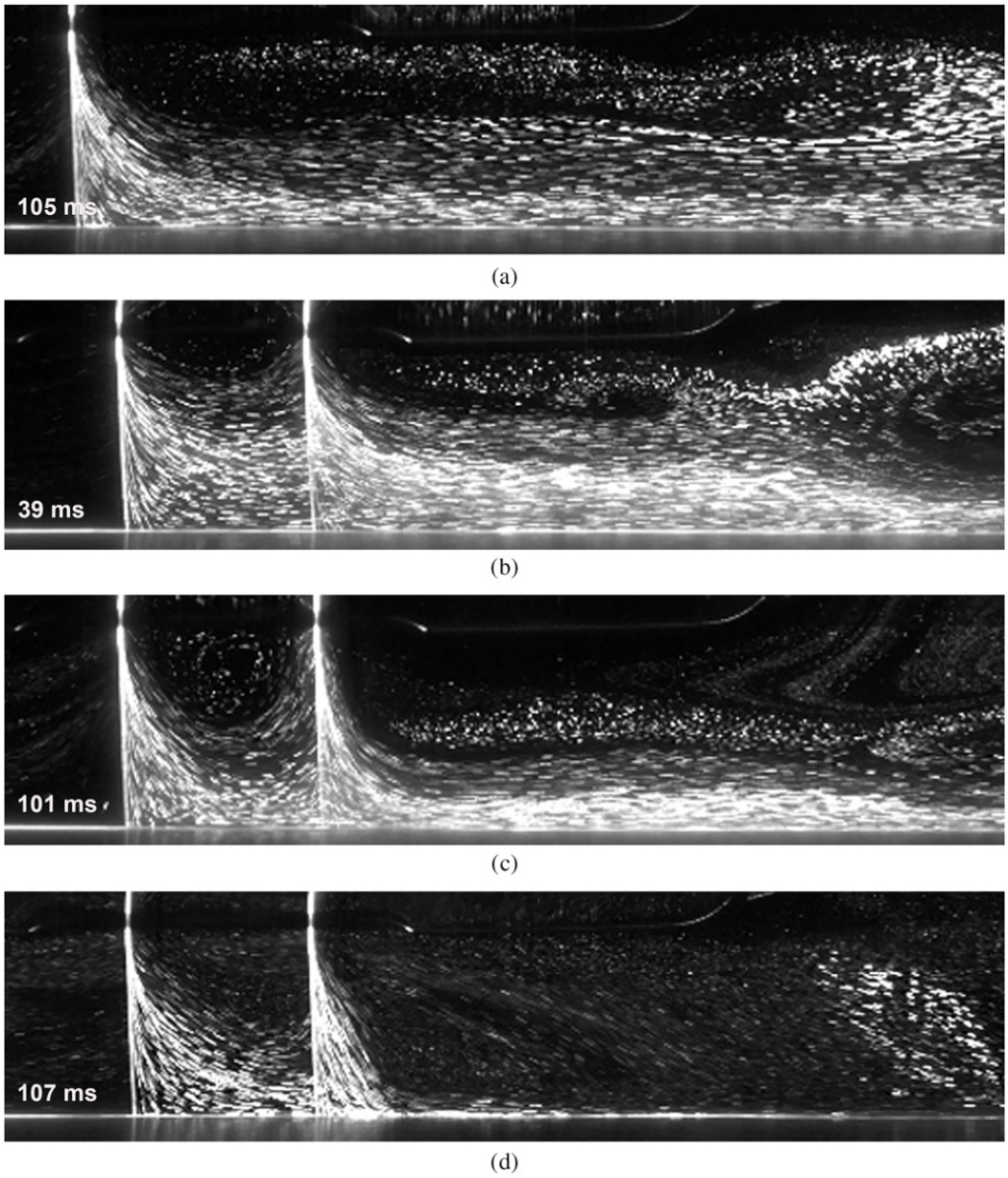

Figure 16. Air and satellite motion for a substrate speed of 1.0 m/s, 13.1 pL droplets, and 5 mm gap. (a) Single row, complete nozzle array (500 lines); (b) two rows, complete nozzle array (1000 lines); (c) two rows, central nozzles (60 lines). The substrate motion was toward the right. Time zero was at the start of printing.

printing frequency and substrate speed. This suggests a possible cause for the repeated misplacement of satellites that produce characteristic patterns commonly referred as "wood-graining" in industrial printing, as seen in Figure 14. This figure shows that the "graining" effect (due to eddy shedding) builds up with time, as there is an initial length of 3–4 cm where it is not visible. This length corresponds to the regime seen in the first image of Fig. 13. Later, when unsteady eddies develop, defects become prevalent and repeated.

Figure 15 shows t-PIV results that provide information about the development and evolution of the eddies, highlighted in red by a vorticity analysis.

Eddy shedding is affected by the substrate speed, as Figures 16 and 17 demonstrate. These images show that when the substrate speed is increased to 1 m/s both the vortex shedding and the graining effect are reduced. This happens for both single-row and two-row printing. Under these conditions, satellites remain as mist under the nozzle plate, and a small eddy upstream of the first printing row is visible, but the formation of eddies downstream is not observed, resulting in better printing quality, as shown in Fig. 17. Entrainment of satellites from neighboring lines is still observed.

These results suggest that avoiding the formation of eddies, particularly those between the printing rows, can produce a less disrupted flow and a more accurate placement of the droplets. This confirms that the less the entrained flow is disrupted, the better are the printing directionality and drop placement. Consequently, an increase in the Couette

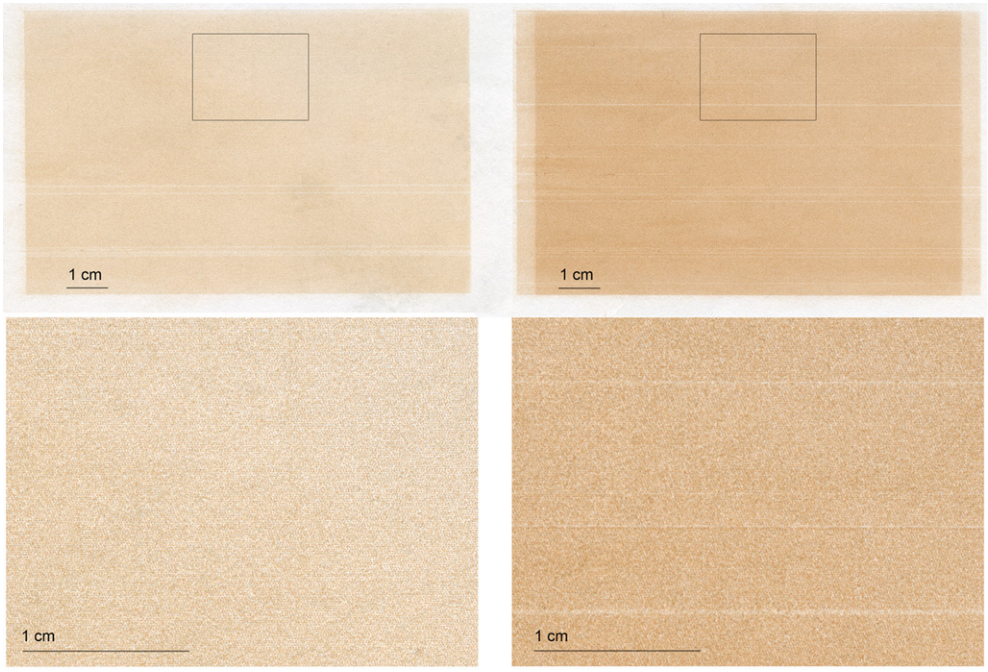

Figure 17. Printed patterns obtained for a substrate speed of 1.0 m/s, 13.1 pL droplets, and 5 mm gap (left: one row; right: two rows). The substrate motion was toward the right. Bottom: the delimited regions are displayed in more detail.

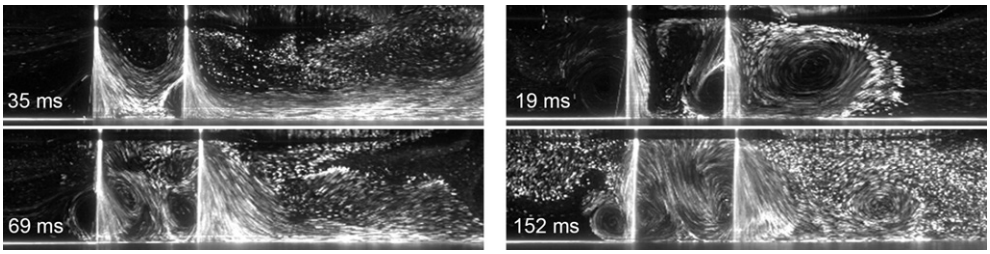

Figure 18. Air and satellite motion for a substrate speed of 1.0 m/s (left) and 0.5 m/s (right) for 63 pL droplets and a 5 mm gap. The substrate motion was toward the right. Time zero was at the start of printing.

flow velocity (larger airflow rate) or an increase of the nozzle spacing gives better printing results.

Printhead B is a gray-scale system which allows the variation of droplet volume. Figure 18 shows the behavior of large droplets (63 pL) for substrate speeds of 1.0 and 0.5 m/s. In comparison with the previous results, eddies formed more readily. The drag exerted by the droplets is now larger, and the wakes alter or interact strongly with the entrained Couette flow and/or between lines. This produces a large number of eddies, being more noticeable at 0.5 m/s (with less drag effect from the entrained Couette flow on the streams of droplets).

Finally, the graining effect is also affected by the gap. Figure 19 shows the formation of eddies with a gap of 1 mm; in this case there is no interaction between them. The printed pattern obtained for droplets of 13 pL volume showed no noticeable misplacement or "wood-graining". In contrast, the formation and interaction between eddies with a gap of 7 mm increased considerably, particularly when the largest droplets were printed. A pattern with larger misplacement faults, similar to that obtained for a 5 mm gap, resulted.

CONCLUSIONS

A visualization technique has been successfully developed and evaluated to study airflows beneath commercial printheads. The new setup is flexible, and it permits the detailed visualization of droplet dynamics with two techniques: laser and shadowgraph illumination. The system offers better quality images of the air and droplet dynamics during printing than those produced by other techniques in previous work. The apparatus can be used to study not only droplet directionality but also satellite mist formation and the aerodynamic effects of substrate roughness, substrate speed variations, printhead shape, and nozzle pitch variations on the quality of printing. Quantitative analysis of droplet and air movement is possible over wide visual fields.

This novel setup involves the use of relatively inexpensive components, and it can allow studies to be carried out

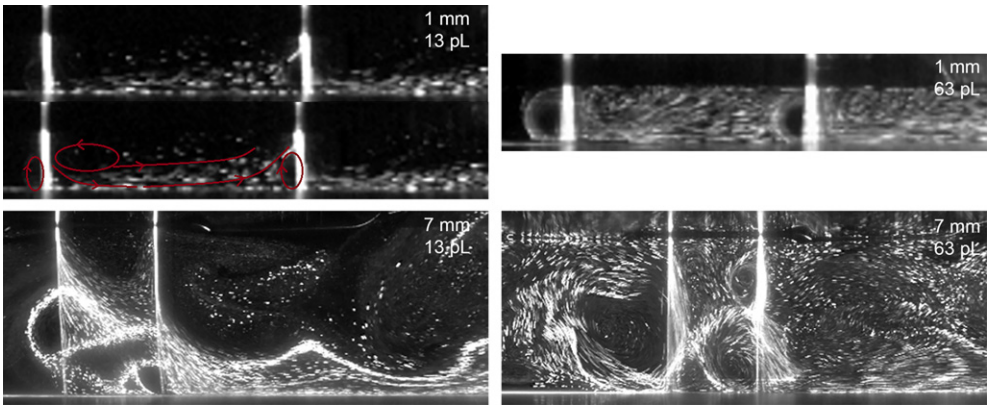

Figure 19. Air and satellite motion for a substrate speed of 0.5 m/s for droplets of 13 pL (left) and 63 pL (right) at a gap of 1 mm (top) and 7 mm (bottom). The substrate motion was toward the right.

from various different viewing angles, for example side and front views, and from above. This system could also be used to study aerodynamic effects due to the addition of external components to the printhead, such as air guards, air blowers, or extractors, which will be the topics of future projects.

It has been demonstrated that drop placement defects are associated with the formation of eddy flows within the gap between the printhead and the moving substrate, and entrainment of satellites generated from neighboring nozzles. Eddies, particularly between sequences of drops ejected from neighboring nozzles, appear in conditions of small nozzle spacing, large gaps, and low substrate speeds. Under these circumstances, the entrained Couette flow is highly distorted. In addition, large droplets generate more violent eddies, since they develop larger drags, which consequently form larger wakes. Greater nozzle spacing and faster substrate speed—a higher entrained airflow rate—enhance the printing quality, by dragging the droplets for a longer length downstream, but without interacting with each other. The use of lateral air guards might be explored as a means to avoid boundary effects.

Other future experiments could focus on changing the external environment to a less dense gas than air in order to reduce drag effects and reduce both the interaction between droplet wakes and the entrained flow, and the generation of wakes.

The data contained in the work is available at: https://www.repository.cam.ac.uk/handle/1810/248294/.

ACKNOWLEDGMENTS

This work was supported by the UK Engineering and Physical Sciences Research Council (Grant EP/H018913/1: Innovation in industrial inkjet technology) and by an EPSRC Impact Acceleration grant from the University of Cambridge (EP/K503757/1).

REFERENCES

[1] N. Link, S. Lampert, R. Gurka, A. Liberzon, G. Hetsroni, and R. Semiat, "Ink drop motion in wide-format printers: II. Airflow investigation," Chem. Eng. Process.: Process Intensification **48**, 84–91 (2009).

[2] W. K. Hsiao, S. D. Hoath, G. D. Martin, and I. M. Hutchings, "Aerodynamic effects in ink-jet printing on a moving web," *Proc. NIP28: 28th Int'l. Conf. on Digital Printing Technologies and Digital Fabrication 2012* (IS&T, Springfield, VA, 2012), pp. 412–415.

[3] W.-K. Hsiao, G. D. Martin, S. D. Hoath, I. M. Hutchings, M. Hook, and M. Massucci, "Evidence of print gap airflow affecting web printing quality," *Proc. NIP29: 29th Int'l. Conf. on Digital Printing Technologies and Digital Fabrication 2013* (IS&T, Springfield, VA, 2013), pp. 303–306.

[4] D. Barnett and M. McDonald, "Evaluation and reduction of elevated height printing defect," *Proc. NIP30: 30th Int'l. Conf. on Digital Printing Technologies and Digital Fabrication 2014* (IS&T, Springfield, VA, 2014), pp. 38–43.

[5] B. Beulen, J. de Jong, H. Reinten, M. van den Berg, H. Wijshoff, and R. van Dongen, "Flows on the nozzle plate of an inkjet printhead," Exp. Fluids **42**, 217–224 (2007).